# Orbit optimization for ASTROD-GW and its time delay interferometry with two arms using CGC ephemeris*

Wang Gang(王 刚)[a)†] and Ni Wei-Tou(倪维斗)[b)c)]

[a)] *Shenzhen National Climate Observatory, No. 1 Qixiang Rd., Zhuzilin, Futian District, Shenzhen 518040, China*

[b)] *Shanghai United Center for Astrophysics (SUCA), Shanghai Normal University, 100 Guilin Road, Shanghai 200234, China*

[c)] *Center for Gravitation and Cosmology (CGC), Department of Physics, National Tsing Hua University, Hsinchu, Taiwan, 300, China*

(Received 25 May 2012; revised manuscript received 13 September 2012)

Astrodynamical space test of relativity using optical devices optimized for gravitation wave detection (ASTROD-GW) is an optimization of ASTROD to focus on the goal of detection of gravitation waves. The detection sensitivity is shifted 52 times toward larger wavelength compared with that of laser interferometer space antenna (LISA). The mission orbits of the three spacecrafts forming a nearly equilateral triangular array are chosen to be near the Sun–Earth Lagrange points *L3*, *L4*, and *L5*. The three spacecrafts range interferometrically with one another with an arm length of about 260 million kilometers. In order to attain the required sensitivity for ASTROD-GW, laser frequency noise must be suppressed to below the secondary noises such as the optical path noise, acceleration noise, etc. For suppressing laser frequency noise, we need to use time delay interferometry (TDI) to match the two different optical paths (times of travel). Since planets and other solar-system bodies perturb the orbits of ASTROD-GW spacecraft and affect the TDI, we simulate the time delay numerically using CGC 2.7 (here, CGC stands for center for gravitation and cosmology) ephemeris framework. To conform to the ASTROD-GW planning, we work out a set of 20-year optimized mission orbits of ASTROD-GW spacecraft starting at June 21, 2028, and calculate the differences in optical path in the first and second generation TDIs separately for one-detector case. In our optimized mission orbits of 20 years, changes of arm lengths are less than 0.0003 AU; the relative Doppler velocities are all less than 3 m/s. All the second generation TDI for one-detector case satisfies the ASTROD-GW requirement.

**Keywords:** orbit optimization, ASTROD-GW, gravitational wave detector, time delay interferometry

**PACS:** 95.10.Eg, 95.55.Ym, 04.80.Nn, 07.60.Ly **DOI:** 10.1088/1674-1056/22/4/049501

## 1. Introduction

The gravitation-wave (GW) experimental groups in the world are actively looking forward to GW detection in the near future.[1,2] The working detectors at present are mainly ground interferometers and pulsar timing arrays (PTAs). The first-generation ground interferometers include LIGO (4-km arm length),[3] Virgo (3-km arm length),[4] GEO (0.6-km arm length),[5] and TAMA (0.3-km arm length).[6] The second-generation ground interferometers under construction are Advanced LIGO,[7] Advanced Virgo,[8] and KAGRA/LCGT (3-km arm length).[9] LIGO-India is under active consideration.[10] KAGRA is an underground detector and its main mirrors will become cryogenic in its second phase to suppress thermal noises. When the second-generation interferometers are completed and their sensitivity goals in the high frequency band (10 Hz–100 kHz; for a classification of GWs, see Refs. [1], [2], and [11]) are achieved in about 5 years, first direct detection of GWs from binary neutron-star mergers, neutron-star/black-hole mergers or black-hole/black-hole mergers will be realized. PTAs seek for the detection of GWs from supermassive black hole merger events and background in the very low frequency band (300 pHz–100 nHz) around 2020.[12]

To detect GWs from various different astrophysical and cosmological sources in different spectral ranges and to enhance the signal-to-noise ratios, we need also to explore the GW spectrum between the high frequency band and the very low frequency band, i.e., the middle frequency band (0.1 Hz–10 Hz) and the low frequency band (100 nHz–0.1 Hz). Space detectors are most sensitive to these bands. Mission concepts under implementation and study are LISA,[13] ASTROD,[14,15] Super-ASTROD,[16] ASTROD–GW,[17,18] BBO,[19] and DECIGO.[20,21] Except for the Fabry–Perot implementation of DECIGO whose scheme is basically like the ground GW interferometric detectors, all other missions have unequal arm lengths and laser frequency noise is very serious. One way to suppress it is to use time delay interferometry (TDI) by combining paths to make the two interfering beams have nearly equal optical paths. Time delay interferometry is considered for ASTROD in 1996[22,23] and has been worked out for LISA much more thoroughly since 1999.[24,25]

With the NASA withdrawal in April 2011, the LISA project was nominally ended. A joint effort from seven European countries (France, Germany, Italy, The Netherlands,

*Project supported by the National Natural Science Foundation of China (Grant Nos. 10778710 and 10875171).

†Corresponding author. E-mail: gwanggw@gmail.com

© 2013 Chinese Physical Society and IOP Publishing Ltd 

Spain, Switzerland, UK) and ESA have made a new proposal eLISA/NGO (evolved Laser Interferometer Space Antenna/New Gravitational Wave Observatory) by down-scaling the size and the arm length of LISA. The mission orbit configuration of three spacecrafts is similar to LISA with the configuration plane inclined by about 60° to the ecliptic, but with nominal arm length $1 \times 10^6$ km (instead of $5 \times 10^6$ km) and the configuration trailing Earth by 10°–20° (instead of around 20°). The mission duration is 2 years for mission (science) orbit (actually, it is about 4 years including transferring and commissioning). eLISA/NGO is one detector with two arms.[26]

Dhurandhar *et al*.[27] have worked out the time delay interferometry observables for LISA for which only the data streams from two arms are considered. These TDI observables could be readily applied to a similar situation for ASTROD-GW (nominal arm length $260 \times 10^6$ km) and to the case of eLISA/NGO which is already a two-arm interferometer. Following the semi-analytical work of Dhurandhar *et al*.,[27] we have worked out these TDI observables in a series of numerical studies of TDIs for LISA (nominal arm length $5 \times 10^6$ km),[28] for eLISA/NGO[29] and for an NGO-LISA-type mission with a nominal arm length of $2 \times 10^6$ km.[29]

In this paper, we work out the time delay interferometry for ASTROD-GW in the case of one-detector two-arm case. In Section 2, we review the ASTROD-GW mission concept. In Section 3, we summarize CGC 2.7 ephemeris framework to be used for optimizing the mission orbit design and to apply to the second-generation TDIs. In Section 4, we optimize the mission orbit of ASTROD-GW to have nearly equal arm lengths and to have minimal line-of-sight Doppler velocity between different pairs of spacecraft for 20 years. In Section 5, we summarize the basics of time-delay interferometry. In Section 6, we work out the second generation TDI for ASTROD-GW with one interferometer. In Section 7, we conclude this paper with discussion. Some of the results of this paper have been reported earlier in an unpublished report and in a master thesis.[30] Part of the results are also used in the comparison of TDIs for eLISA/NGO, for an NGO-LISA-type mission with a nominal arm length of $2 \times 10^6$ km, for LISA and for ASTROD-GW.[29]

## 2. ASTROD-GW

ASTROD-GW is an optimization of ASTROD to focus on the goal of detection of GWs.[1,11,17,18] The scientific aim is focused on GW detection at low frequency. The mission orbits of the three spacecrafts forming a nearly equilateral triangular array are chosen to be near the Sun–Earth Lagrange points $L3$, $L4$, and $L5$ (Fig. 1).

The three spacecrafts range interferometrically with one another with an arm length of about 260 million kilometers. After a first mission-orbit optimization,[31–33] the changes of the three arm lengths are all less than 0.0003 AU or, fractionally, less than $\pm 1.7 \times 10^{-4}$ in ten years, and the Doppler velocities for the three spacecrafts are all less than ±4 m/s. These parameters are consistent with those of LISA requirement and, therefore, a number of technologies developed by LISA could be applied to ASTROD-GW also. For the purpose of primordial GW detection, a 6-S/C (S/C: spacecraft) formation for ASTROD-GW will be used for correlated detection of stochastic GWs.[1,11,17,18]

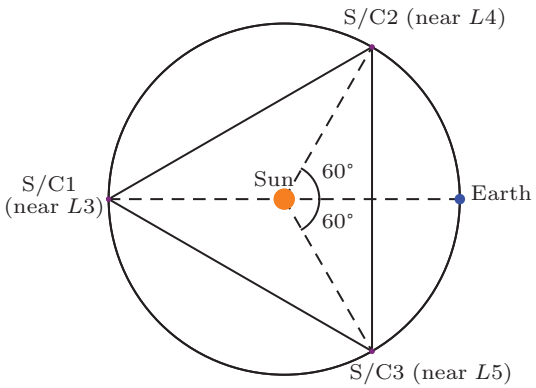



**Fig. 1.** (color online) Schematic plot of ASTROD-GW mission orbit design.

Since the arm length is 52 times longer than that of LISA, with (1–2) W laser power and LISA acceleration noise, the strain sensitivity of ASTROD-GW is 52 times lower than that of LISA, and is better than those of LISA and Pulsar Timing Arrays (PTAs) in the frequency band of 100 nHz–1 mHz. The sensitivity curve for ASTROD-GW as compared with LISA is shown in Fig. 2.[11] With longer arm length, the requirement for the power of weak light phase locking is more stringent for ASTROD-GW. In the cases of LISA and eLISA/NGO, their powers are around 100 pW and 1 nW respectively; in the case of ASTROD-GW, it is in the range of 50 fW–100 fW. We have demonstrated the weak light phase locking capability to 2 pW.[34,35] More recently, Jet Propulsion Laboratory (JPL) people have demonstrated the weak light phase locking capability to 40 fW.[36] The power requirement feasibility of phase locking is met. ASTROD-GW will complement eLISA/NGO and PTA in exploring black hole co-evolution with galaxies and GW backgrounds in an important frequency range of 100 nHz–1 mHz.

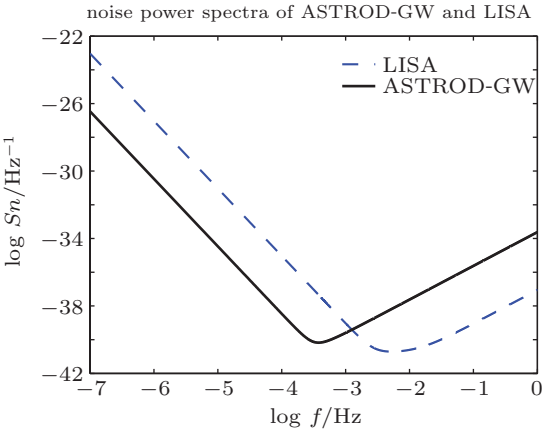



**Fig. 2.** (color online) ASTROD-GW strain noise power spectrum as compared with LISA strain noise power spectrum.

## 3. CGC ephemeris

In 1998, we started orbit simulation and parameter determination for ASTROD.[37,38] We worked out a post-Newtonian ephemeris of the Sun including the solar quadrupole moment, the major planets and three biggest asteroids. We term this working ephemeris CGC 1. Using this ephemeris as a deterministic model and adding stochastic terms to simulate noise, we generated simulated ranging data and used Kalman filtering to determine the accuracies of fitted relativistic and solar-system parameters for 1050 days of the ASTROD mission.

For a better evaluation of the accuracy of $\dot{G}/G$, we need also to monitor the masses of other asteroids. For this, we considered all known 492 asteroids with diameter greater than 65 km to obtain an improved ephemeris framework — CGC 2, and calculated the perturbations due to these 492 asteroids on the ASTROD spacecraft.[39,40]

In building a CGC ephemeris framework, we use the post-Newtonian barycentric metric and equations of motion as derived in Brumberg[41] with parameterized post-Newtonian (PPN) parameters $\beta$ and $\gamma$ for solar system bodies. For an introduction to post-Newtonian approximation, please see Refs. [42] and [43]. The metric with the setting gauge parameter $\alpha$ to be zero is

$$\begin{aligned} ds^2 &= \left[1-2\sum_i \frac{m_i}{r_i}+2\beta\left(\sum_i \frac{m_i}{r_i}\right)^2\right. \\ &\quad +(4\beta-2)\sum_i \frac{m_i}{r_i}\sum_{j\neq i}\frac{m_j}{r_{ij}} \\ &\quad -c^{-2}\sum_i \frac{m_i}{r_i}\left(2(\gamma+1)\dot{\boldsymbol{x}}_i^2-\boldsymbol{r}_i\cdot\ddot{\boldsymbol{x}}_i-\frac{1}{r_i^2}(\boldsymbol{r}_i\cdot\dot{\boldsymbol{x}}_i)^2\right) \\ &\quad \left.+\frac{m_1R_1^2}{r_1^3}J_2\left(3\,(\frac{\boldsymbol{r}_1\cdot\hat{\boldsymbol{z}}}{r_1})^2-1\right)\right]c^2dt^2 \\ &\quad +2c^{-1}\sum_i \frac{m_i}{r_i}((2\gamma+2)\dot{\boldsymbol{x}}_i)\cdot d\boldsymbol{x}cdt \\ &\quad -\left[1+2\gamma\sum_i \frac{m_i}{r_i}\right](d\boldsymbol{x})^2, \end{aligned} \tag{1}$$

where $\boldsymbol{r}_i=\boldsymbol{x}-\boldsymbol{x}_i$, $\boldsymbol{r}_{ij}=\boldsymbol{x}_i-\boldsymbol{x}_j$, $m_i=GM_i/c^2$, $M_i$ is the mass of the body with $M_1$ the solar mass,[41] $J_2$ is the quadrupole moment parameter of the Sun, $\hat{\boldsymbol{z}}$ is the unit vector normal to the elliptic plane. The associated equations of motion of N-mass problem as derived from the geodesic variational principle of this metric are

$$\begin{aligned} \ddot{\boldsymbol{x}}_i &= -\sum_{j\neq i}\frac{GM_j}{r_{ij}^3}\boldsymbol{r}_{ij}+\sum_{j\neq i}m_j(A_{ij}\boldsymbol{r}_{ij}+B_{ij}\dot{\boldsymbol{r}}_{ij}), \\ A_{ij} &= \frac{\dot{\boldsymbol{x}}_i^2}{r_{ij}^3}-(\gamma+1)\frac{\dot{r}_{ij}^2}{r_{ij}^3}+\frac{3}{2r_{ij}^5}(\boldsymbol{r}_{ij}\dot{\boldsymbol{x}}_j)^2 \\ &\quad +G[(2\gamma+2\beta+1)M_i+(2\gamma+2\beta)M_j]\frac{1}{r_{ij}^4} \\ &\quad +\sum_{k\neq i,j}GM_k\left[(2\gamma+2\beta)\frac{1}{r_{ij}^3r_{ik}}+(2\beta-1)\frac{1}{r_{ij}^3r_{jk}}\right. \\ &\quad \left.+\frac{2(\gamma+1)}{r_{ij}r_{jk}^3}-\left(2\gamma+\frac{3}{2}\right)\frac{1}{r_{ik}r_{jk}^3}-\frac{1}{2r_{jk}^3}\frac{\boldsymbol{r}_{ij}\boldsymbol{r}_{ik}}{r_{ij}^3}\right], \\ B_{ij} &= \frac{1}{r_{ij}^3}[(2\gamma+2)(\boldsymbol{r}_{ij}\dot{\boldsymbol{r}}_{ij})+(\boldsymbol{r}_{ij}\dot{\boldsymbol{x}}_j)]. \end{aligned} \tag{2}$$

These equations are used to build our computer-integrated ephemeris (with $\gamma=\beta=1$, $J_2=2\times10^{-7}$) for eight-planets, the Pluto, the Moon, and the Sun. The positions and velocities at the epoch (at 0:00 on 10 June 2005), were taken from the DE403 ephemeris. The evolution is solved by using the 4th-order Runge–Kutta method with the step size $h=0.01$ day. In Ref. [37] the 11-body evolution is extended to 14-body to include the three big asteroids — Ceres, Pallas, and Vesta (CGC 1 ephemeris). Since the tilt of the axis of the solar quadrupole moment with respect to the normal of the elliptical plane is small (7°), in CGC 1 ephemeris, we have neglected this tilt. In CGC 2 ephemeris, we have added the perturbations of an additional 489 asteroids.

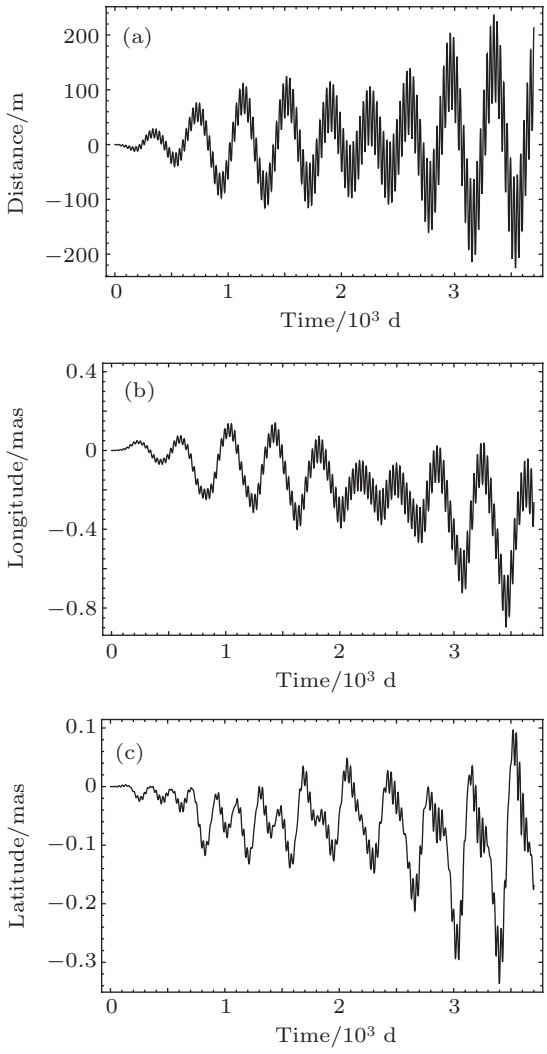



**Fig. 3.** Differences (DE405-CGC2.7) in (a) radial distance, (b) longitude, (c) latitude starting at JD2461944.0 between Earth orbits in DE405 and CGC 2.7 ephemerides in the J2000 Heliocentric Earth mean equatorial coordinate system.

In our previous optimization of ASTROD-GW orbits,[31–33] we have used CGC 2.5 ephemeris in which only the three biggest minor planets were taken into account, but the Earth's precession and nutation were added; the solar quadratic zonal harmonic and the Earth's quadratic to quartic zonal harmonic were considered.

In this paper, we add the perturbation of an additional 349 asteroids and call it CGC 2.7 ephemeris.

The differences in orbit evolution compared with DE405 for Earth for 3700 days starting at JD2461944.0 (at 12:00:00 on 21 June 2028) are shown in Fig. 3. The differences in radial distance are less than about 200 m.

## 4. Mission orbit optimization

The goal of ASTROD-GW mission orbit optimization is to equalize the three arm lengths of ASTROD-GW formation and to reduce the relative line-of-sight velocities between three pairs of spacecrafts as much as possible. In our previous optimization, the start time of the science part of the mission is chosen to be 21 June 2025 (JD2460848.0) and the optimization is for a period of 3700 days.[31–33] The preparation of the mission may take a longer time and there is a potential that the extended mission life time may be longer than 10 years, so in this paper, we start at noon on June 21, 2028 (JD2461944.0) and perform the optimization for a period of 20 years by following our previous method.

### 4.1. Initial choice of spacecraft initial conditions

A possible launch time for ASTROD-GW is in the latter part of the 2020s. For the sake of definiteness we choose noon, on 21 June 2028 (JD2461944.0) as the initial epoch for the mission orbit. Another choice of the initial epoch also has similar solutions. Since the dominant force on the spacecraft is from the Sun in the restricted three-body problem of Earth–Sun–spacecraft system. To start the optimization, the initial positions of the three spacecrafts can be chosen to form an equilateral triangle on 1-AU solar orbit and the initial velocity is chosen to follow an orbit period of one sidereal year. To fix the orbit phases of the three spacecrafts, we notice that $L4$ and $L5$ Lagrange points of Sun–Earth system are stable and $L3$ Lagrange point is mildly unstable with time constant about 50 years. For a mission of 10–20 years, $L3$ point is actually quasi-stable. Therefore, we choose the initial positions of three spacecrafts in the heliocentric ecliptic coordinate system to be S/C1 at (0, 1 AU, 0), S/C2 at ($3^{1/2}2^{-1}$ AU, $-0.5$ AU, 0), S/C3 at ($-3^{1/2}2^{-1}$ AU, $-0.5$ AU, 0). S/C1 is near $L3$ point, S/C2 near $L4$ point, S/C3 near $L5$ point. Since the Earth–Sun orbit is elliptical, the Lagrange points are not stationary. However, the spacecrafts are in the halo orbits of the respective Lagrange points, largely compensating the non-stationary motions of the Lagrange points to remain nearly circular orbits of the Sun. The initial velocities of the three spacecrafts in the heliocentric ecliptic coordinate system are chosen to be S/C1 at ($-v_0$, 0, 0), S/C2 at (0.5 $v_0$, $3^{1/2}2^{-1}$ $v_0$, 0), S/C3 at (0.5 $v_0$, $-3^{1/2}2^{-1}$ $v_0$, 0), where $v_0$ (= 0.01720209895 AU/day) is the circular velocity of spacecraft at 1 AU from the Sun.

The initial positions and initial velocities of the three spacecrafts in J2000 equatorial solar-system–barycentric coordinate system are listed in the third column of Table 1 which also lists the initial conditions for an intermediate step (after period optimization) and for final results in our optimization for easy comparison.

**Table 1.** Initial states of S/Cs at epoch JD2461944.0 for our initial choice, after period optimization, and after all optimizations in J2000 equatorial solar-system–barycentric coordinate system.

| | | Initial choice of S/Cs initial states | Initial states of S/Cs after period optimization | Initial states of S/Cs after final optimization |
|---|---|---|---|---|
| S/C1 | $X$ | $1.15400625657242\times10^{-3}$ | $1.15400625657242\times10^{-3}$ | $1.15400625657242\times10^{-3}$ |
| Position | $Y$ | $9.15264788418969\times10^{-1}$ | $9.15261701184544\times10^{-1}$ | $9.15289225648841\times10^{-1}$ |
| AU | $Z$ | $3.96855707171320\times10^{-1}$ | $3.96854368692135\times10^{-1}$ | $3.96866302001196\times10^{-1}$ |
| S/C1 | $V_x$ | $-1.72009645137827\times10^{-2}$ | $-1.72008300146903\times10^{-2}$ | $-1.72003163872199\times10^{-2}$ |
| Velocity | $V_y$ | $4.88112077380618\times10^{-6}$ | $4.88112077380618\times10^{-6}$ | $4.88112077380618\times10^{-6}$ |
| (AU/d) | $V_z$ | $2.07014410548162\times10^{-6}$ | $2.07014410548162\times10^{-6}$ | $2.07014410548162\times10^{-6}$ |
| S/C2 | $X$ | $8.67179410041011\times10^{-1}$ | $8.67179419751799\times10^{-1}$ | $8.67153438989685\times10^{-1}$ |
| Position | $Y$ | $-4.60958426468166\times10^{-1}$ | $-4.60958432557285\times10^{-1}$ | $-4.60944670325136\times10^{-1}$ |
| AU | $Z$ | $-1.99809745830377\times10^{-1}$ | $-1.99809748470332\times10^{-1}$ | $-1.99803781815802\times10^{-1}$ |
| S/C2 | $V_x$ | $8.60218391121732\times10^{-3}$ | $8.60233950755836\times10^{-3}$ | $8.60259754371050\times10^{-3}$ |
| Velocity | $V_y$ | $1.36730297780320\times10^{-2}$ | $1.36730847422802\times10^{-2}$ | $1.36734947883888\times10^{-2}$ |
| (AU/d) | $V_z$ | $5.92793451120697\times10^{-3}$ | $5.92795834111164\times10^{-3}$ | $5.92813611775755\times10^{-3}$ |
| S/C3 | $X$ | $-8.64871397527866\times10^{-1}$ | $-8.64871407921666\times10^{-1}$ | $-8.64862747667628\times10^{-1}$ |
| Position | $Y$ | $-4.60958426468166\times10^{-1}$ | $-4.60958431471891\times10^{-1}$ | $-4.60953844061175\times10^{-1}$ |
| AU | $Z$ | $-1.99809745830377\times10^{-1}$ | $-1.99809747999756\times10^{-1}$ | $-1.99807759114913\times10^{-1}$ |
| S/C3 | $V_x$ | $8.60218391121732\times10^{-3}$ | $8.60233303252539\times10^{-3}$ | $8.60242121981651\times10^{-3}$ |
| Velocity | $V_y$ | $-1.36632675364844\times10^{-2}$ | $-1.36633074545593\times10^{-2}$ | $-1.36634452887228\times10^{-2}$ |
| (AU/d) | $V_z$ | $-5.92379422299601\times10^{-3}$ | $-5.92381152958984\times10^{-3}$ | $-5.92387128797985\times10^{-3}$ |

### 4.2. Method of optimization

In the solar system, the ASTROD-GW spacecraft orbits are perturbed by the other planets. The largest perturbation is caused by Jupiter and Venus. Therefore the orbital period and the eccentricity change. Our method of optimization is to modify the initial velocities and initial heliocentric distances so that the perturbed orbital periods for ten- or twenty-year average remain close to sidereal year and the average eccentricity remains near zero.

The total orbital energy (kinetic and potential) of a planet around the Sun for two-body problem is given by

$$E = \frac{mv^2}{2} - \frac{G(M+m)m}{r} = -\frac{G(M+m)m}{2a}. \tag{3}$$

The sidereal orbital period of planet is

$$T = \frac{2\pi a^{3/2}}{\sqrt{G(M+m)}}. \tag{4}$$

Here, $G$ is the gravitational constant, $M$ is the mass of Sun, $m$ is the planetary mass, $v$ is the orbital velocity of the planet, $r$ the planetary heliocentric distance and $a$ is the semi-major axis of planetary orbit.

#### 4.2.1. Trimming the period

For ASTROD-GW spacecraft, the orbit is nearly circular and we have $r \approx a$. From Eq. (3), we have

$$v^2 \approx \frac{G(M+m)}{r} \approx \frac{G(M+m)}{a}. \tag{5}$$

Two useful expressions between orbital period and velocity, and orbital period and position can be found from Eqs. (4) and (5) to be

$$\begin{aligned} \Delta v &= -\frac{1}{3}\frac{\Delta T}{T} v, \\ \Delta r &= \frac{2}{3}\frac{\Delta T}{T} r. \end{aligned} \tag{6}$$

Actually, we use Eq. (6) as

$$\begin{aligned} \boldsymbol{V}_{\rm new} &= \boldsymbol{V}_{\rm prev} + \Delta\boldsymbol{V} \approx \left(1 - \frac{1}{3}\frac{\Delta T}{T}\right)\boldsymbol{V}_{\rm prev}, \\ \boldsymbol{R}_{\rm new} &= \boldsymbol{R}_{\rm prev} + \Delta\boldsymbol{R} \approx \left(1 + \frac{2}{3}\frac{\Delta T}{T}\right)\boldsymbol{R}_{\rm prev}, \end{aligned} \tag{7}$$

where $\boldsymbol{V}_{\rm prev}$ and $\boldsymbol{R}_{\rm prev}$ are the velocity and position of spacecraft before adjusting, $\Delta T$ is the variation of the orbital period wanted, $\boldsymbol{V}_{\rm new}$ and $\boldsymbol{R}_{\rm new}$ are the new initial conditions with new period.

#### 4.2.2. Eccentricity trimming

From Eq. (4), we notice that the orbital period $T$ is determined by the semi-major axis $a$. Keeping the period means fixing $a$. From Eq. (3), the method of adjusting the eccentricity to keep the period fixed gives

$$\frac{\Delta v}{v} = -\frac{\Delta r}{r}. \tag{8}$$

To trim the eccentricity we need to change the initial velocity and initial radial distance using

$$\begin{aligned} \boldsymbol{V}_{\rm new} &= \boldsymbol{V}_{\rm prev} + \Delta\boldsymbol{V} \approx \left(1 - \frac{\Delta R}{R}\right)\boldsymbol{V}_{\rm prev}, \\ \boldsymbol{R}_{\rm new} &= \boldsymbol{R}_{\rm prev} + \Delta\boldsymbol{R} \approx \left(1 + \frac{\Delta R}{R}\right)\boldsymbol{R}_{\rm prev}, \end{aligned} \tag{9}$$

where $R$ is the initial heliocentric distance of spacecraft and the change $\Delta R$ is to induce the variation of eccentricity wanted.

### 4.3. Optimization steps

At the beginning of an optimization step, we calculate the orbits of the spacecraft from initial conditions using the ephemeris CGC 2.7. From these orbits, we calculate the mean orbital period in 20 years, the variations of arm length, differences between arm lengths, heliocentric distances of spacecraft, and Doppler velocities between spacecrafts each as a function of mission time.

With these data, we use Eq. (7) to optimize the orbital period of each spacecraft. (i) We first calculate the average period of each spacecraft and change the initial conditions to match the periods to one sidereal year to minimize the change of arm lengths. (ii) Due to planetary perturbations, for the spacecraft near $L3$ point, the period decreases slightly as time goes on, while for the spacecraft near $L4$ and $L5$ points, the period increases slightly as time goes on; Arm 3 changes from shorter to longer, Arm 2 changes from longer to shorter, and the Arm 1 changes are relatively small. In this situation, we reduce the initial velocity of S/C1 to let the initial period be slightly longer; and we increase the initial velocities of S/C2 and S/C3 to let their initial period be slightly shorter. In this way, we can compensate the period deviation tendency of the three spacecrafts, and minimize the period differences and arm length differences dynamically. After trimming the period, the arm length differences are decreased; however, in general, the orbit configuration still does not satisfy mission requirements.

In the next step, we use Eq. (9) to trim the S/C eccentricities into being nearly circular, until initial heliocentric distance becomes close to perihelion or aphelion distance.

In the general case, after application of these two steps once, the ASTROD-GW requirements would still not be satisfied. Repeated applications of period and eccentricity optimizations are needed to satisfy the requirements. The initial conditions obtained after period optimization, and after all optimizations are listed, for comparison, in columns 4 and 5 of Table 1 in the J2000 equatorial solar-system-barycentric coordinate system. The variations of arm lengths, difference of arm lengths, angles between arms, and velocities in the line-of-sight direction are drawn for 20 years in Fig. 4.

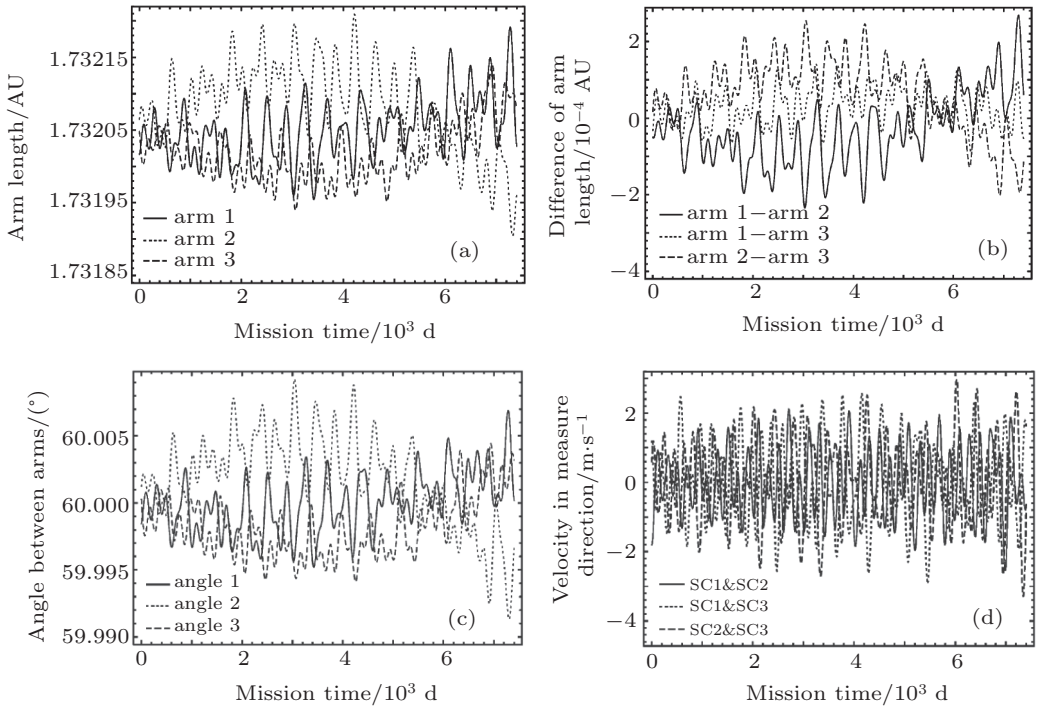



**Fig. 4.** Variations of (a) arm lengths, (b) difference between arm lengths, (c) angles between arms, and (d) velocities in the measurement direction in 20 years.

The index label of the arm is defined by the index of the opposite spacecraft, and the index label of the angle is the same as the index of the spacecraft.

## 5. Time-delay interferometry (TDI)

For laser-interferometric antenna for space detection of GWs, the arm length varies according to orbit dynamics. In order to attain the required sensitivity, laser frequency noise must be suppressed to below the secondary noises such as the optical path noise, acceleration noise, etc. For suppressing laser frequency noise, TDI is needed to match the optical path length of different beams. The better the match of the optical path lengths is, the better the cancellation of the laser frequency noise is and the easier it is to achieve the required sensitivity. In the case of exact match, the laser frequency noise is fully cancelled, as indicated in the original Michelson interferometer.

In the study of ASTROD mission concept, the TDI was first used.[22,23,44] In the deep-space interferometry, long distances are invariably involved. Due to long distances, laser light is attenuated to a great extent at the receiving spacecraft. To transfer the laser light back or to another spacecraft, amplification is needed. The procedure is to phase lock the local laser to the incoming weak laser light and to transmit the local laser back to another spacecraft. We have demonstrated in the laboratory the phase locking of a local oscillator with 2-pW laser light.[34,35] Dick *et al*.[36] have demonstrated phase locking to 40-fW incoming weak laser light. The power requirement feasibility for ASTROD-GW is met with these developments. In the 1990s, we used the following two TDI configurations during the study of ASTROD interferometry and obtained numerically the path length differences using the following Newtonian dynamics:[22,23,44]

i) unequal arm Michelson TDI Configuration

Path 1: $\mathrm{S/C1} \to \mathrm{S/C2} \to \mathrm{S/C1} \to \mathrm{S/C3} \to \mathrm{S/C1}$,

Path 2: $\mathrm{S/C1} \to \mathrm{S/C3} \to \mathrm{S/C1} \to \mathrm{S/C2} \to \mathrm{S/C1}$;

ii) Sagnac TDI configuration:

Path 1: $\mathrm{S/C1} \to \mathrm{S/C2} \to \mathrm{S/C3} \to \mathrm{S/C1}$,

Path 2: $\mathrm{S/C1} \to \mathrm{S/C3} \to \mathrm{S/C2} \to \mathrm{S/C1}$.

Here we do the same thing for ASTROD-GW. For the numerical evaluation, we take a common receiving time epoch for both beams; the results would be very close to each other numerically if we take the same start time epoch and calculate the path differences. The results of this calculation are shown in Fig. 5. We refer to the path $\mathrm{S/C1} \to \mathrm{S/C2} \to \mathrm{S/C1}$ as $a$ and the path $\mathrm{S/C1} \to \mathrm{S/C3} \to \mathrm{S/C1}$ as $b$. Hence the difference between Path 1 and Path 2 for the unequal-arm Michelson can be denoted as $ab - ba \equiv [a, b]$.

Time delay interferometry has been investigated for LISA much more thoroughly since 1999.[24,25] First-generation and

second-generation TDIs are proposed. In the first generation TDIs, static situations are considered, while in the second generation TDIs, motions are compensated to a certain degree. The two configurations considered above and results shown in Fig. 5 are for first generation TDI configurations according to Tinto and Dhurandhar,[25] although in the calculations dynamics is used. We shall not review more about these historical developments here, but the readers may refer to the excellent review by Tinto and Dhurandhar[25] for comprehensive treatment.

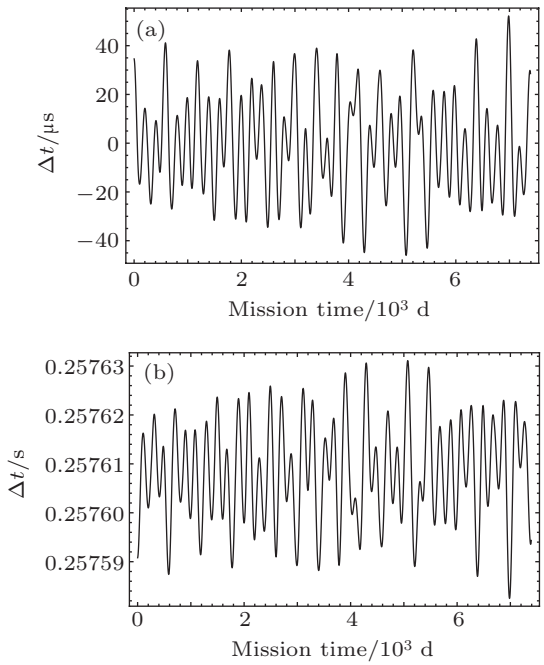



**Fig. 5.** Path length differences between two optical paths for (a) unequal-arm Michelson TDI configuration, i.e., [$a$, $b$] and (b) Sagnac configuration.

In the following section, we will work out the path length differences of second-generation TDIs numerically for the two-arm case of ASTROD-GW.

## 6. Second-generation TDI for ASTROD-GW

The second-generation TDIs obtained by Dhurandhar *et al.*[27] are listed in degree-lexicographic order as follows:

(I) $n = 1$, $[ab, ba] = abba - baab$,

(II) $n = 2$, $[a^2b^2, b^2a^2]$, $[abab, baba]$; $[ab^2a, ba^2b]$,

(III) $n = 3$, $[a^3b^3, b^3a^3]$, $[a^2bab^2, b^2aba^2]$, $[a^2b^2ab, b^2a^2ba]$, $[a^2b^3a, b^2a^3b]$, $[aba^2b^2, bab^2a^2]$, $[ababab, bababa]$, $[abab^2a, baba^2b]$, $[ab^2a^2b, ba^2b^2a]$, $[ab^2aba, ba^2bab]$, $[ab^3a^2, ba^3b^2]$, lexicographic (binary) order.

For the numerical evaluation, we take a common receiving time epoch for both beams and calculate the path differences. Figures 6–8 show the numerical results for the $n = 1$, $n = 2$, and $n = 3$ TDI configurations respectively.

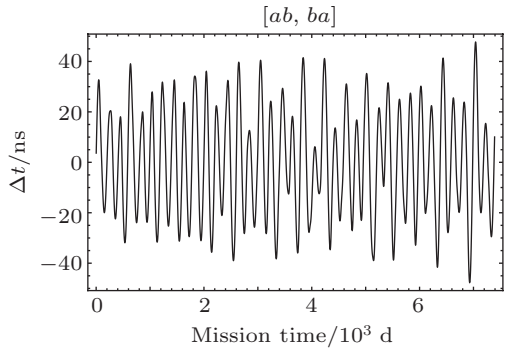



**Fig. 6.** Path length difference between two optical paths of $n = 1$ TDI configuration.

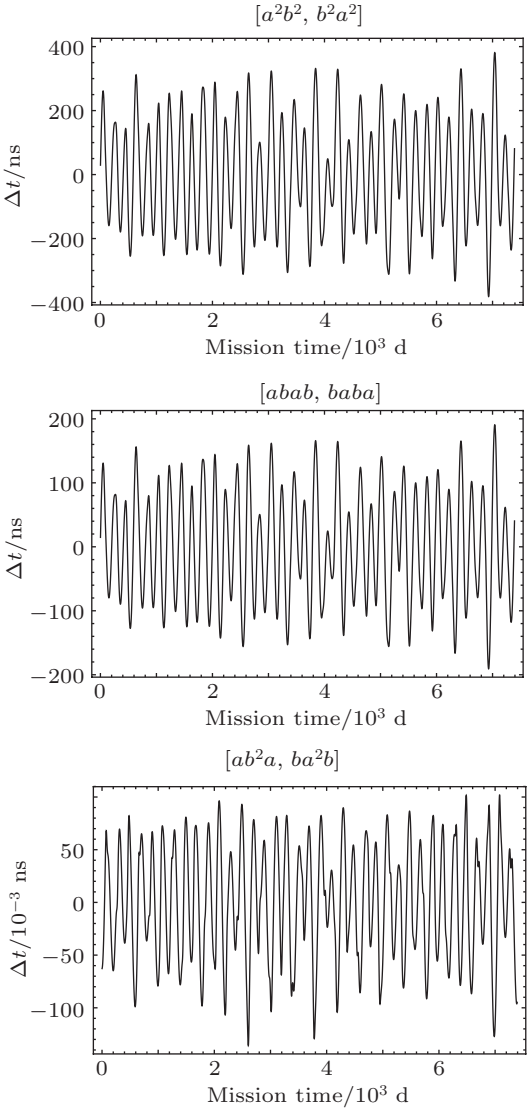



**Fig. 7.** Path length differences between two optical paths of three $n = 2$ TDI configurations.

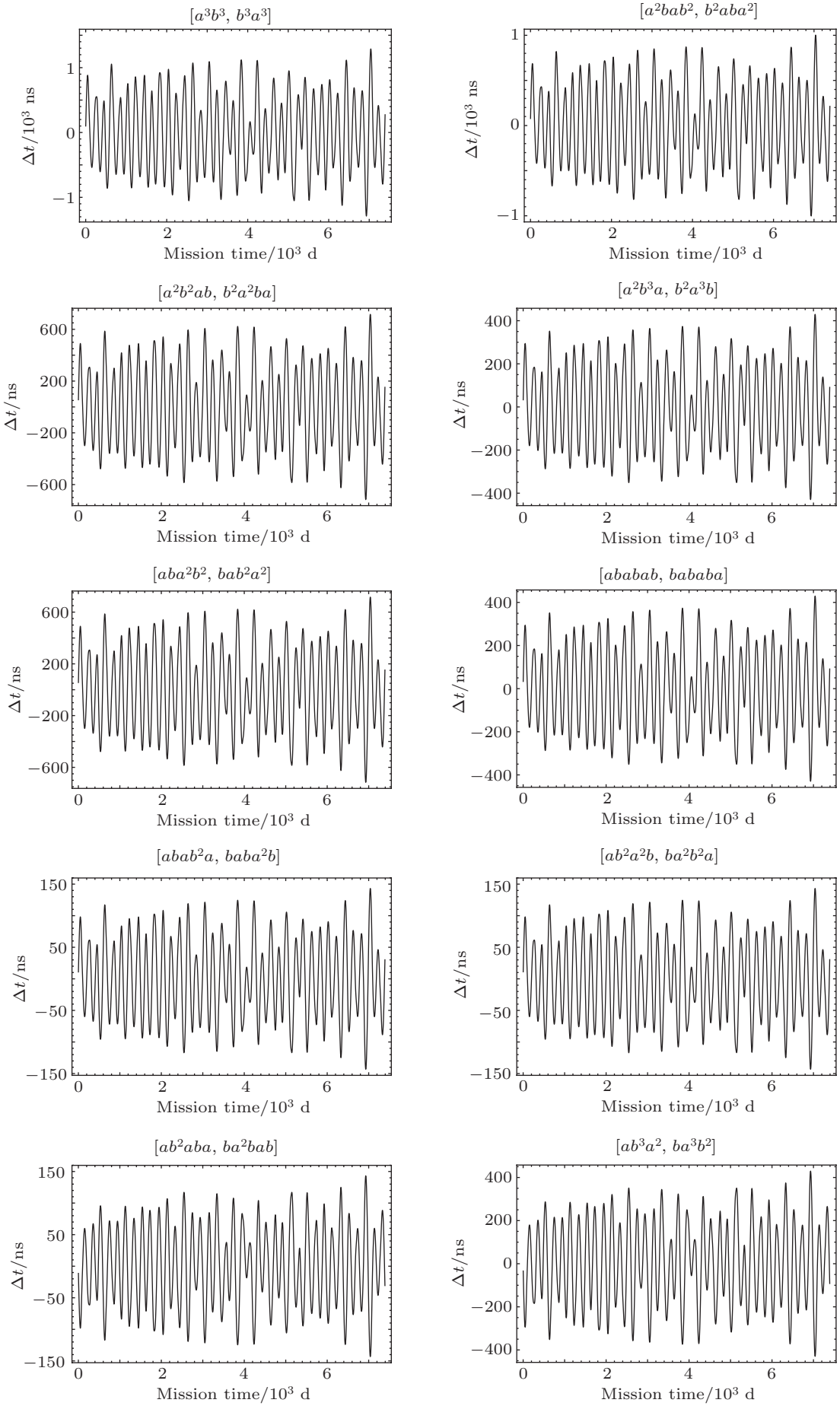



**Fig. 8.** Path length differences between two optical paths of ten $n = 3$ TDI configurations.

## 7. Discussions

In the ASTROD-GW mission for detecting GWs in a frequency range of 100 nHz–100 mHz, the three spacecrafts range interferometrically with one another with an arm length of about 260 million kilometers in between. After optimization of orbits, changes of arm lengths can all be less than 0.0003 AU and the relative Doppler velocities can be less than 3 m/s for 20 years of mission. In order to attain the required sensitivity for ASTROD-GW, laser frequency noise must be suppressed to below the secondary noises such as the optical path noise, acceleration noise, etc. For suppressing the laser frequency noise, we use time delay interferometry to match the time (optical path length). To conform to the ASTROD-GW planning, we work out a set of 20-year optimized mission orbits of ASTROD-GW spacecraft starting from 21 June 2028, and calculate the residual errors in the first and second generation time delay interferometry. All the second generation time delay interferometry calculated in this paper satisfies the ASTROD-GW requirement (less than 500 m).

In this paper, except for Sagnac TDI configuration, we only consider one-detector two-arm cases. Other first-generation numerical TDI solutions and some of the second-generation numerical TDI solutions for full three arms have been worked out in Refs. [45] and [46]. Comparisons with TDIs for eLISA/NGO and LISA in Ref. [29] are discussed.

## References


[1] Ni W T 2010 *Mod. Phys. Lett. A* **25** 922
[2] Classification of Gravitational Waves http://astrod.wikispaces.com/file/view/GW-classification.pdf
[3] The LIGO Scientific Collaboration, http://www.ligo.caltech.edu/
[4] The Virgo Collaboration, http://www.virgo.infn.it/
[5] The GEO600 Team, http://geo600.aei.mpg.de
[6] TAMA300 Collaboration, http://tamago.mtk.nao.ac.jp/
[7] The Advanced LIGO Team, http://www.ligo.caltech.edu/advLIGO/
[8] The Advanced Virgo Team, http://wwwcascina.virgo.infn.it/advirgo/
[9] KAGRA Large-scale Cryogenic Gravitational Wave Telescope Project, http://gwcenter.icrr.u-tokyo.ac.jp/en/
[10] Indigo, http://www.gw-indigo.org
[11] Ni W T 2013 *Adv. Space Res.* **51** 525
[12] Demorest P, Lazio J and Lommen A, *et al*. 2009 arXiv: 0902.2968 [astro-ph]
[13] LISA Study Team 2000 LISA (Laser Interferometer Space Antenna): A Cornerstone Mission for the Observation of Gravitational Waves, ESA *System and Technology Study Report* ESA-SCI (2000) 11
[14] Bec-Borsenberger A, Christensen-Dalsgaard J, Cruise M, Di Virgilio A, Gough D, Keiser M, Kosovichev A, Laemmerzahl C, Luo J, Ni W T, Peters A, Samain E, Scherrer P H, Shy J T, Touboul P, Tsubono K, Wu A M Yeh H C 2000 *Astrodynamical Space Test of Relativity Using Optical Devices ASTROD—A Proposal Submitted to ESA in Response to Call for Mission Proposals for Two Flexi-Mission F2/F3*
[15] Ni W T 2008 *Int. J. Mod. Phys. D* **17** 921
[16] Ni W T 2009 *Class. Quantum Grav.* **26** 075021
[17] Ni W T 2009 ASTROD Optimized for Gravitational-wave Detection: ASTROD-GW — A Pre-Phase A Study Proposal Submitted to Chinese Academy of Sciences, February 26, 2009
[18] Ni W T, Men J R and Mei X H, *et al*. 2009 *Proceedings of Sixth Deep Space Exploration Technology Symposium,* December 3–6, 2009 Sanya, China, p. 122
[19] Crowder J and Cornish N J 2005 *Phys. Rev. D* **72** 083005
[20] Kawamura S, Nakamura T and Ando M, *et al*. 2006 *Class. Quantum Grav*. **23** S125
[21] Kawamura S, Ando M and Seto N, *et al.* 2011 *Class. Quantum Grav.* **28** 094011
[22] Ni W T, Shy J T, Tseng S M, Xu X, Yeh H C, Hsu W Y, Liu W L, Tzeng S D, Fridelance P, Samain E and Wu A M 1997 *Proceedings of SPIE* 3116: *Small Spacecraft, Space Environments, and Instrumentation Technologies*, p. 105
[23] Ni W T, Sandford M C W, Veillet C, Wu A M, Fridelance P, Samain E, Spalding G and Xu X 2003 *Adv. Space Res.* **32** 1437
[24] Armstrong J W, Estabrook F B and Tinto M 1999 *Astrophys. J.* **527** 814
[25] Tinto M and Dhurandhar S V 2005 *Living Rev. Relativity* **8** 4
[26] eLISA/NGO Assessment Study Team, ESA/SRE [2011]19, http://elisa-ngo.org/
[27] Dhurandhar S V, Nayak K R and Vinet J Y 2010 *Class. Quantum Grav.* **27** 135013
[28] Dhurandhar S V, Ni W T and Wang G 2013 *Adv. Space Res.* **51** 198
[29] Wang G and Ni W T 2012 arXiv: 1204.2125v1 [gr-qc]
[30] Wang G 2011 Time-delay Interferometry for ASTROD-GW (MS Thesis), (Nanjing: Purple Mountain Observatory) (in Chinese)
[31] Men J R, Ni W T and Wang G 2009 *Proceedings of Sixth Deep Space Exploration Technology Symposium*, December 3–6, 2009 Sanya, China, p. 47
[32] Men J R, Ni W T and Wang G 2009 *Acta Astron. Sin.* **51** 198 (in Chinese)
[33] Men J R, Ni W T and Wang G 2010 *Chin. Astron. Astrophys.* **34** 434
[34] Liao A C, Ni W T and Shy J T 2002 *Publications of the Yunnan Observatory* **3** 88
[35] Liao A C, Ni W T and Shy J T 2002 *Int. J. Mod. Phys. D* **11** 1075
[36] Dick G J, Strekalov M D and Birnbaum K, *et al*. 2008 *IPN Progress Report* **42** 175
[37] Chiou D W and Ni W T 2000 *Adv. Space Res.* **25** 1259
[38] Chiou D W and Ni W T 2000 arXiv: 0407570 [astro-ph]
[39] Tang C J and Ni W T 2000 arXiv: 0407606 [astro-ph]
[40] Tang C J and Ni W T 2002 *Publications of the Yunnan Observatory* **3** 21 (in Chinese)
[41] Brumberg V A 1991 *Essential Relativistic Celestial Mechanics* (Bristol: Adam Hilger) p. 175
[42] Misner C W, Thorne K S and Wheeler J A 1973 *Gravitation* (San Francisco: Freeman)
[43] Yi Z 2002 "*Relativistic Celestial Mechanics and Post-Newtonian Equations of Motion*", *Publications of the Yunnan Observatory* **3** 9 (in Chinese)
[44] Ni W T 1997 *Gravitational Wave Detection* (Tokyo: Universal Academy Press) p. 117
[45] Wang G and Ni W T 2011 *Acta Astron. Sin.* **52** 427 (in Chinese)
[46] Wang G and Ni W T 2012 *Chin. Astron. Astrophys.* **36** 211